NUMERICAL MATHEMATICS: Theory, Methods and Applications
Numer. Math. Theor. Meth. Appl., Vol. **1**, No. 3, pp. 275-296 (2008)

A $\mathbb{P}_N \times \mathbb{P}_N$ Spectral Element Projection Method for the Unsteady Incompressible Navier-Stokes Equations

Zhijian Rong and Chuanju Xu*

School of Mathematical Sciences, Xiamen University, 361005 Xiamen, China.

Received 14 August, 2007; Accepted (in revised version) 28 November, 2007

Abstract. In this paper, we present a $\mathbb{P}_N \times \mathbb{P}_N$ spectral element method and a detailed comparison with existing methods for the unsteady incompressible Navier-Stokes equations. The main purpose of this work consists of: (i) detailed comparison and discussion of some recent developments of the temporal discretizations in the frame of spectral element approaches in space; (ii) construction of a stable $\mathbb{P}_N \times \mathbb{P}_N$ method together with a $\mathbb{P}_N \to \mathbb{P}_{N-2}$ post-filtering. The link of different methods will be clarified. The key feature of our method lies in that only one grid is needed for both velocity and pressure variables, which differs from most well-known solvers for the Navier-Stokes equations. Although not yet proven by rigorous theoretical analysis, the stability and accuracy of this one-grid spectral method are demonstrated by a series of numerical experiments.

AMS subject classifications: 65N35, 74S25, 76D07

Key words: $\mathbb{P}_N \times \mathbb{P}_N$, Navier-Stokes equations, spectral element methods.

1. Introduction

There have been numerous studies on the numerical approximation and its applications to the Navier-Stokes equations (NSE) since the past century. The Navier-Stokes equations have some features that make the construction of numerical method difficult. For example, the coupling of the velocity and pressure in the NSE brings a great difficulty in the numerical simulation of incompressible flows.

Generally, there are two principal ways to deal with this coupling in the time-dependent NSE. One way is to first keep the velocity and pressure coupled at the level of time discretization leading to a generalized Stokes problem, and then to apply the so-called Uzawa algorithm to the resulting algebraic system once the generalized Stokes problem is discretized in space. The Uzawa algorithm employs a block Gauss elimination in the discrete saddle-point problem to decouple the velocity from the pressure and yields two positive definite symmetric systems: one for the velocity and the other for the pressure (see e.g. [20] and the references therein). This decoupling procedure has been proven to be more attractive than a direct algorithm, however the classical Uzawa algorithm suffers

*Corresponding author. *Email addresses:* zjrong@xmu.edu.cn (Z. Rong), cjxu@xmu.edu.cn (C. Xu)

from expensive computation of the pressure system as the pressure matrix involves the inverses of the Helmholtz systems. This disadvantage has been overcome by using an additional splitting technique, termed occasionally as “matrix factorization" [13], leading to a Poisson-like equation for the pressure. This approach has a common foundation with traditional projection-like splitting approaches which give a Poisson equation for the pressure except that, in the former case, the splitting is effected in the discrete form of the equations. Such an approach was analyzed and applied to several computations in the papers of Perot [22], Couzy *et al.* [7] and Fischer [10], but no rigorous error estimate in time is available. We will term here this kind of methods as Uzawa-based method. The disadvantage of the Uzawa-based method is that a discrete form of the Ladyshenskaya-Brezzi-Babuška condition (LBB condition, see e.g. [5]) must be satisfied for obtaining the unique discrete solution. The well-known $\mathbb{P}_N \times \mathbb{P}_{N-2}$ spectral element method (SEM), introduced in [21], addresses this problem through the use of compatible velocity and pressure spaces that are free of pressure spurious modes. There exist however some methods that make use other space pairs than $\mathbb{P}_N \times \mathbb{P}_{N-2}$, we refer to [3,6] for a detailed description of these methods.

Projection-type methods, introduced first by Chorin [8,9] and Temam [27] in the late 1960s, give another way to decouple the velocity and the pressure in the computation of unsteady incompressible flows. They are based on a particular time-discretization of the equations governing viscous incompressible flows, in which the viscosity and the incompressibility of the fluid are dealt within two separate steps. By doing that, the original problem is reformulated into two simpler problems. The projection algorithm can be classed into two families: classical fractional step methods and pressure-correction methods. The classical fractional step methods have only first order convergence rate due to the fact that they are basically an artificial compressibility technique [23,24]. Unlike Uzawa-based methods that preserve the original pressure boundary conditions, projection-type methods introduce implicitly new pressure boundary conditions. The inconsistent pressure boundary conditions usually give rise to numerical instability or/and reduce the accuracy of the scheme. Different choices of the pressure boundary condition have been discussed to improve the efficiency of this kind of methods (see [18] for instance). In a standard pressure-correction scheme the pressure accuracy can be at most of first-order in the L^2-norm, as shown by Strikwerda and Lee in [25]. Later, a modified pressure-correction scheme was introduced by Timmermans, Minnev and Van De Vosse [26], and analyzed by Guermond and Shen [15] in the semi-discrete form and by Huang and Xu [17] in the full discrete form. Optimal error estimates have been obtained [17] by assuming that the discrete velocity and pressure space pair satisfies the LBB condition. The role of the LBB conditions in the frame of the projection-type schemes has been an issue for a long time. We refer to [2,14] for recent detailed discussions in this sense. It should be emphasized that from the point of view of implementation, the LBB condition between the velocity and the pressure approximation space is not mandatory for the projection methods to work. Indeed, a principal interest in using the projection-type method is that we are free from the compatibility restriction on the choice of the discrete velocity and pressure space. Otherwise, the Uzawa-based method [7,10,19,22,29] could be the preference.

From the theoretical point of view, it is well-known that the LBB condition is a nec-

essary and sufficient condition to obtain the optimal convergence rate when the velocity and the pressure are formulated in a coupled form. This is because that the well-known spurious modes (see, e.g., [4]) may pollute the pressure if the LBB condition is violated. However, when solving the velocity and the pressure in two decoupled steps by the projection schemes, there is no evidence showing that the LBB condition is a necessary condition to guarantee the uniqueness of the pressure solution. Although numerical pressure oscillations using $\mathbb{P}_N \times \mathbb{P}_N$ spectral projection methods with very small time steps were recently reported [2], it seems to us that the cause of these oscillations is not yet clear.

In the paper, we attempt to provide further analysis to the above mentioned problems, and try to clarify some points. Especially, we will introduce a simple $\mathbb{P}_N \times \mathbb{P}_N$ method with no need to use staggered grid. The method is based on the projection schemes, together with a $\mathbb{P}_N \to \mathbb{P}_{N-2}$ post-filtering. Numerical tests show that this $\mathbb{P}_N \times \mathbb{P}_N$ method removes the numerical pressure oscillations found in the traditional $\mathbb{P}_N \times \mathbb{P}_N$ projection methods.

The rest of the paper will be organized as follows. First, we provide in Section 2 a review on the temporal-spatial discretizations of the time-dependent Stokes equations in the frame of spectral element methods. In Section 3 we propose a one-grid stable $\mathbb{P}_N \times \mathbb{P}_N$ spectral method. Numerical tests will be presented suitably in different sections to demonstrate the efficiency of the proposed method. Some concluding remarks are given at the end of the paper.

2. Time-dependent Stokes equations and discretizations

For ease of notation, hereafter we use letters of boldface to denote vectors or vector functions. We consider the following time-dependent Stokes equations written in terms of the primitive variables: given the forcing term $\boldsymbol{f}(t,\boldsymbol{x})$ and divergence-free initial velocity $\boldsymbol{u}_0$, find a velocity field $\boldsymbol{u}$ and a pressure field p such that

$$\begin{cases} \partial_t \boldsymbol{u} - \nu \nabla^2 \boldsymbol{u} + \nabla p = \boldsymbol{f} & \text{in } \Omega \times (0,T], \\ \nabla \cdot \boldsymbol{u} = 0 & \text{in } \Omega \times (0,T], \\ \boldsymbol{u}|_{\partial\Omega} = 0 & \text{in } (0,T], \\ \boldsymbol{u}|_{t=0} = \boldsymbol{u}_0 & \text{in } \Omega, \end{cases} \tag{2.1}$$

where Ω is an open connected bounded domain of $\mathcal{R}^d, d = 2,3$, with a piecewise smooth boundary $\partial\Omega$, ν is the kinematic viscosity. For the sake of simplicity, here we assume that the velocity $\boldsymbol{u}$ is prescribed with homogeneous boundary conditions.

It is well known that a principle difficulty on the numerical solution of the problem (2.1) is due to the coupling of the velocity and the pressure in the momentum equation. This difficulty has led to much investigation. Generally, there are two ways to decouple this coupling: Uzawa-based algorithm and projection-type schemes. In this section, we try to compare these two decoupling techniques and attempt to provide insights to improve both approaches. To simplify the presentation, we limit ourselves to the case of second order schemes, although higher order schemes can be compared in a similar way.

Firstly, we define some functional spaces endowed with standard norms and inner products. In particular, we define the spaces

$$H^1(\Omega)=\{v\in L^2(\Omega),\nabla v\in L^2(\Omega)^d\ \},$$
$$H_0^1(\Omega)=\{v\in H^1(\Omega),\ v=0\ on\ \partial\Omega\},$$
$$L_0^2(\Omega)=\{v\in L^2(\Omega),\int_\Omega v d\boldsymbol{x}=0\},$$

where $L^2(\Omega)$ is the space of measurable functions whose square is Lebesgue integrable in Ω. The inner products of $L^2(\Omega)$ and $H^1(\Omega)$ are defined by

$$(u,v)_\Omega=\int_\Omega uv\mathrm{d}\boldsymbol{x},\ \ (u,v)_{1,\Omega}=(u,v)_\Omega+(\nabla u,\nabla v)_\Omega,\ \ u,v\in L^2(\Omega),$$

and the corresponding norms by

$$\|v\|_\Omega=\sqrt{(v,v)_\Omega},\ \ \|v\|_{1,\Omega}=\sqrt{(v,v)_{1,\Omega}}.$$

For vector functions, we define

$$(\boldsymbol{u},\boldsymbol{v})_\Omega=\int_\Omega\sum_{i=1}^d u_iv_i\ \mathrm{d}\boldsymbol{x},\ \ \|\boldsymbol{u}\|_\Omega^2=\int_\Omega\sum_{i=1}^d u_i^2\ \mathrm{d}\boldsymbol{x},\ \ \boldsymbol{u},\boldsymbol{v}\in L^2(\Omega)^d.$$

Hereafter, in cases where no confusion would arise, the domain symbol Ω may be dropped from the notations.

To present spectral element discretization, we assume that domain Ω has been partitioned into E conform quadrangles (in 2D) or hexahedrons (in 3D), such that

$$\bar\Omega=\bigcup_{e=1}^E\bar\Omega_e,\quad \Omega_i\bigcap\Omega_j=\varnothing,\ \ if\ i\neq j.$$

Let $\hat\Omega$ be the reference domain, i.e., $\hat\Omega=\Lambda^2$ (in 2D) or $\hat\Omega=\Lambda^3$ (in 3D), where $\Lambda=(-1,1)$. $\boldsymbol{f}^e$ is a one-to-one continuous mapping from the reference domain $\hat\Omega$ to the physical domain Ω_e. We denote by $I\!P_{N,E}(\Omega)$ the piecewise polynomial space:

$$I\!P_{N,E}(\Omega)=\{v_N\in L^2(\Omega);v_N|_{\Omega_e}\circ\boldsymbol{f}^e\in I\!P_N(\hat\Omega),1\le e\le E\},$$

where $I\!P_N(\hat\Omega)$ is the space of all polynomials of degree at most N with respect to each variable.

Let ξ_i,ω_i $(i=0,\cdots,N)$ be the N-Gauss-Lobatto-Legendre (GLL(N) or simply GLL if there is no possible confusion) quadrature points and weights in the reference interval $\bar\Lambda$, such that

$$\int_{-1}^1 v dx=\sum_{i=0}^N v(\xi_i)\omega_i,\quad \forall v\in I\!P_{2N-1}(\Lambda).$$

We denote by $h_i, 0 \le i \le N$, the Lagrangian interpolants based on the GLL points $\{\xi_i\}_{0\le i\le N}$.

Let ζ_j, ρ_j $(j = 1, \cdots, N-1)$ be the $(N-2)$-Gauss-Legendre (GL$(N-2)$ or GL) quadrature points and weights, such that

$$\int_{-1}^{1} v dx = \sum_{i=1}^{N-1} v(\zeta_i)\rho_i, \ \forall v \in I\!P_{2N-3}(\Lambda).$$

We denote by $l_i, 1 \le i \le N-1$, the Lagrangian interpolants based on the GL points $\{\zeta_i\}_{1\le i\le N-1}$. We define the quadrature points and weights in Ω_e by the mapping $\boldsymbol{f}^e$, that is:

$$\begin{aligned}
&\xi^e_{ijk} := \boldsymbol{f}^e(\xi_i, \xi_j, \xi_k), \ \ \omega^e_{ijk} = J_e(\xi_i, \xi_j, \xi_k)\omega_i\omega_j\omega_k, \ \ i,j,k = 0,1,\cdots,N;\\
&\zeta^e_{ijk} := \boldsymbol{f}^e(\zeta_i, \zeta_j, \zeta_k), \ \ \rho^e_{ijk} = J_e(\zeta_i, \zeta_j, \zeta_k)\rho_i\rho_j\rho_k, \ \ i,j,k = 1,2,\cdots,N-1,
\end{aligned}$$

where J_e is the Jacobian determinant of the mapping $\boldsymbol{f}^e$. Then we have the following GLL numerical integral approximation

$$\begin{aligned}
(u,v)_{\Omega_e} &= \int_{\hat{\Omega}} u\circ\boldsymbol{f}^e v\circ\boldsymbol{f}^e J_e d\boldsymbol{x}\\
&\approx \sum_{i,j,k=0}^{N} u\circ\boldsymbol{f}^e(\xi_i,\xi_j,\xi_k) v\circ\boldsymbol{f}^e(\xi_i,\xi_j,\xi_k) J_e(\xi_i,\xi_j,\xi_k)\omega_i\omega_j\omega_k\\
&= \sum_{i,j,k=0}^{N} u(\xi^e_{ijk}) v(\xi^e_{ijk})\omega^e_{ijk}\ ;
\end{aligned}$$

or its GL counterpart

$$(u,v)_{\Omega_e} \approx \sum_{i,j,k=1}^{N-1} u(\zeta^e_{ijk}) v(\zeta^e_{ijk})\rho^e_{ijk}\ .$$

These approximations lead us to define the GLL L^2-discrete inner product, $\forall u, v \in C^0(\Omega)$,

$$(u,v)_{\mathcal{N},GL} = \sum_{e=1}^{E}(u,v)_{\Omega_e,GL}, \ \text{with}\ (u,v)_{\Omega_e,GL} = \sum_{i,j,k=0}^{N} u(\xi^e_{ijk}) v(\xi^e_{ijk})\omega^e_{ijk}\ , \tag{2.2}$$

and the GL L^2-discrete inner product

$$(u,v)_{\mathcal{N},G} = \sum_{e=1}^{E}(u,v)_{\Omega_e,G}, \ \text{with}\ (u,v)_{\Omega_e,G} = \sum_{i,j,k=1}^{N-1} u(\zeta^e_{ijk}) v(\zeta^e_{ijk})\rho^e_{ijk}\ , \tag{2.3}$$

where we use $\mathcal{N}$ to denote the parameter pair (N,E). The definitions of the discrete inner products for vector functions are similar to that for scalar functions.

Finally we define the spaces:

$$X_{\mathcal{N}} = H^1_0(\Omega)^d \cap I\!P_{N,E}(\Omega)^d, \quad M_{\mathcal{N}} = I\!P_{N-2,E}(\Omega) \cap L^2_0(\Omega).$$

2.1. Uzawa algorithm and matrix factorization

In view of comparison with the $\mathbb{P}_N \times \mathbb{P}_N$ spectral method that we are going to introduce in next section, we first recall the classical $\mathbb{P}_N \times \mathbb{P}_{N-2}$ methods. One classical way to discretize problem (2.1) in time is to use the backward differentiation (BD). The second order BD schema reads

$$\begin{cases} \dfrac{3\boldsymbol{u}^{n+1}-4\boldsymbol{u}^{n}+\boldsymbol{u}^{n-1}}{2\triangle t}-\nu\triangle\boldsymbol{u}^{n+1}+\nabla p^{n+1}=\boldsymbol{f}^{n+1} & \text{in } \Omega, \\ \nabla\cdot\boldsymbol{u}^{n+1}=0 & \text{in } \Omega, \\ \boldsymbol{u}^{n+1}=0 & \text{on } \partial\Omega. \end{cases} \tag{2.4}$$

To alleviate the notation, we will hereafter omit index $n+1$ from the dependent and independent variables of the current time step. With this convention, (2.4) can be rewritten into form

$$\begin{cases} \alpha\boldsymbol{u}-\nu\triangle\boldsymbol{u}+\nabla p=\boldsymbol{s} \ \text{ in } \Omega, \\ \nabla\cdot\boldsymbol{u}=0 \ \text{ in } \Omega, \\ \boldsymbol{u}=0 \ \text{ on } \partial\Omega, \end{cases} \tag{2.5}$$

where

$$\alpha=\frac{3}{2\triangle t}, \quad \boldsymbol{s}=\boldsymbol{f}^{n+1}+\frac{1}{2\triangle t}(4\boldsymbol{u}^{n}-\boldsymbol{u}^{n-1}).$$

The spectral element approximation to problem (2.5) reads: find $\boldsymbol{u}_{\mathcal{N}} \in X_{\mathcal{N}}, p_{\mathcal{N}} \in M_{\mathcal{N}}$, such that

$$\begin{cases} a_{\mathcal{N}}(\boldsymbol{u}_{\mathcal{N}},\boldsymbol{v}_{\mathcal{N}})+b_{\mathcal{N}}(p_{\mathcal{N}},\boldsymbol{v}_{\mathcal{N}})=(\boldsymbol{s},\boldsymbol{v}_{\mathcal{N}})_{\mathcal{N},GL}, & \forall \boldsymbol{v}_{\mathcal{N}} \in X_{\mathcal{N}}, \\ b_{\mathcal{N}}(q_{\mathcal{N}},\boldsymbol{u}_{\mathcal{N}})=0, & \forall q_{\mathcal{N}} \in M_{\mathcal{N}}, \end{cases} \tag{2.6}$$

where

$$a_{\mathcal{N}}(\boldsymbol{u}_{\mathcal{N}},\boldsymbol{v}_{\mathcal{N}})=\alpha(\boldsymbol{u}_{\mathcal{N}},\boldsymbol{v}_{\mathcal{N}})_{\mathcal{N},GL}+\nu(\nabla\boldsymbol{u}_{\mathcal{N}},\nabla\boldsymbol{v}_{\mathcal{N}})_{\mathcal{N},GL}, \tag{2.7}$$

$$b_{\mathcal{N}}(q_{\mathcal{N}},\boldsymbol{v}_{\mathcal{N}})=(q_{\mathcal{N}},\nabla\cdot\boldsymbol{v}_{\mathcal{N}})_{\mathcal{N},G}. \tag{2.8}$$

This is the so-called $\mathbb{P}_N \times \mathbb{P}_{N-2}$ method, one of the most popular SEM for the Stokes equations.

By expressing $\boldsymbol{u}_{\mathcal{N}}$ in terms of the Lagrangian interpolants based on the elemental GLL points, $p_{\mathcal{N}}$ in terms of the Lagrangian interpolants based on the elemental GL points, then choosing each test function $\boldsymbol{v}_{\mathcal{N}}$ and $q_{\mathcal{N}}$ to be nonzero at only one global collocation point, we derive from (2.6):

$$\begin{cases} H\underline{u}_i-D_i^TB\underline{p}=\bar{B}\underline{s}_i, \ \ i=1,\cdots,d, \\ BD_i\underline{u}_i=\underline{0}, \end{cases} \tag{2.9}$$

where the underlines denote nodal value vectors, for example,

$$\underline{p}=\{p_{\mathcal{N}}(\zeta_{ijk}^{e})\}_{1\le e\le E;1\le i,j,k\le N-1},$$

and $\underline{u}_i$'s are the components of $\underline{\boldsymbol{u}}$, i.e., $\underline{\boldsymbol{u}} = (\underline{u}_1, \cdots, \underline{u}_d)$. The other notations in (2.9) are defined as follows (for simplification we consider here $E = 1$; in case $E > 1$ there will be a need to use the so-called "stiffness summation" notation to deal with the inter-element C^0 continuity, see, e.g., [21]):

• $\boldsymbol{D}^T := (D_1, \cdots, D_d)^T$ is the matrix form of the discrete gradient operator, defined by

$$\begin{aligned}(D_1)_{ijk,lmn} &:= D_{il} I_{jm} I_{kn},\\ (D_2)_{ijk,lmn} &:= I_{il} D_{jm} I_{kn},\\ (D_3)_{ijk,lmn} &:= I_{il} I_{jm} D_{kn},\end{aligned}$$

where $(D_{pq})_{1\le p\le N-1, 0\le q\le N}, D_{pq} = h'_q(\zeta_p)$, is the GLL→GL derivative matrix, $(I_{pq})_{1\le p\le N-1, 0\le q\le N}, I_{pq} = h_q(\zeta_p)$, is the interpolation matrix, mapping nodal values from GLL points to GL points.

• $\boldsymbol{D} = (D_1, \cdots, D_d)$ is the divergence matrix. The action of $\boldsymbol{D}$ on the GLL nodal values of a given vector function results in the GL nodal values of the divergence of this function.

• B is the GL quadrature mass matrix: $diag(\rho_{ijk})$.

• $\bar{B}$ is the GLL quadrature mass matrix: $diag(\omega_{ijk})$.

• H is the Helmholtz matrix: $H = \alpha\bar{B} + \nu A$, where A is the Laplace matrix, i.e., $A = \bar{D}_j^T \bar{B} \bar{D}_j$, with $\bar{D}_1, \cdots, \bar{D}_d$, defined by

$$\begin{aligned}(\bar{D}_1)_{ijk,lmn} &:= \bar{D}_{il}\delta_{jm}\delta_{kn},\\ (\bar{D}_2)_{ijk,lmn} &:= \delta_{il}\bar{D}_{jm}\delta_{kn},\\ (\bar{D}_3)_{ijk,lmn} &:= \delta_{il}\delta_{jm}\bar{D}_{kn},\end{aligned}$$

where $(\bar{D}_{pq})_{0\le p\le N, 0\le q\le N}, \bar{D}_{pq} = h'_q(\xi_p)$, is the GLL→GLL derivative matrix, δ_{pq} is the Kronecker symbol.

It is at this level, Uzawa algorithm is applied to yield two separated systems:

$$(BD_i H^{-1} D_i^T B)\underline{p} = -BD_i H^{-1} \bar{B}\underline{s}_i, \tag{2.10}$$

$$H\underline{u}_i = D_i^T B\underline{p} + \bar{B}\underline{s}_i, \quad i = 1, \cdots, d. \tag{2.11}$$

The advantage of the Uzawa algorithm is that the computation of the pressure and the velocity is now completely decoupled. A disadvantage of this algorithm is also obvious: the system in the discrete pressure $\underline{p}$ involves the inverse H^{-1}. The computational cost of solving the pressure system can be heavy if an iterative method, such as conjugate gradient iteration, is considered. To overcome this difficulty, several authors proposed and analyzed an additional factorization step to reduce the system (2.9), see for instance [10, 19, 22]. The idea is to recast (2.9) into an equivalent form as follows

$$\begin{cases} H\underline{u}_i - \alpha^{-1}(H\bar{B}^{-1}D_i^T B)(\underline{p} - \underline{p}^n) = \bar{B}\underline{s}_i + D_i^T B\underline{p}^n + \underline{r}_i, \quad i = 1, \cdots, d,\\ BD_i\underline{u}_i = \underline{0}\,, \end{cases} \tag{2.12}$$

where $\underline{p}^n$ is the pressure calculated at t^n. Consequently, $\delta\underline{p} := \underline{p} - \underline{p}^n$ represents the pressure increment between the current time step $n+1$ and time step n. The residual $\underline{r}_i$ takes form:

$$\underline{r}_i = (I - \alpha^{-1}H\bar{B}^{-1})D_i^T B\delta\underline{p}, \quad i = 1, \cdots, d.$$

Neglecting $\underline{\boldsymbol{r}}$ in (2.12) and using the Uzawa algorithm give:

$$\alpha^{-1}(BD_i\bar{B}^{-1}D_i^TB)\delta\underline{p} = -BD_iH^{-1}(\bar{B}\underline{s}_i + D_i^TB\underline{p}^n), \tag{2.13}$$

$$H(\underline{u}_i - \alpha^{-1}\bar{B}^{-1}D_i^TB\delta\underline{p}) = \bar{B}\underline{s}_i + D_i^TB\underline{p}^n, \quad i = 1,\cdots,d. \tag{2.14}$$

Although no rigorous proof is available, formally this is a method of 2nd order in time. This can be seen by taking into account the fact that $\alpha^{-1} = \mathcal{O}(\triangle t), \delta\underline{p} = \mathcal{O}(\triangle t)$. Then a direct calculation shows that

$$\underline{r}_i = -\alpha^{-1}\nu A\bar{B}^{-1}D_i^TB\delta\underline{p} = \mathcal{O}(\triangle t^2).$$

Since there is a factor of $\triangle t^{-1}$ in front of the velocity in (2.12), the local truncation error is $\mathcal{O}(\triangle t^3)$. This analysis is confirmed by the numerical test presented in Fig. 1, where the errors of the velocity and the pressure in various norms are plotted as a function of the time step. In this test, the computational domain is the unit square, with spectral element number $E = 1$. The polynomial degree N has been taken large enough in order to ensure that the spatial error is negligible as compared to the temporal error. Clearly, the errors show an decay of second order in the time step $\triangle t$.

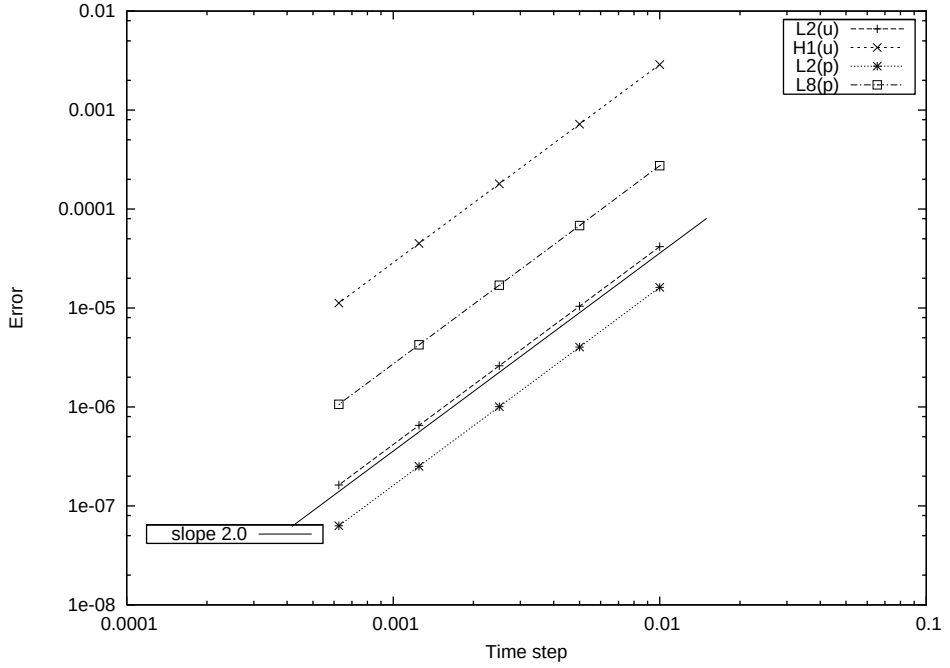

Figure 1: Temporal accuracy of the matrix factorization approach of the Uzawa algorithm.

Remark 2.1. *$\boldsymbol{r}$ decreases as ν decreases. As a result, the error introduced by the factorization step becomes smaller for problems of high Reynolds number (or small viscosity).*

By comparing (2.10) and (2.13), it is seen that the pressure system matrix $BD_iH^{-1}D_i^TB$ in (2.10) has been reduced to $BD_i\bar{B}^{-1}D_i^TB$ in (2.13) by the factorization approach. Simplification of the latter is obvious thanks to the fact that the inversion of the diagonal matrix $\bar{B}$ is much cheaper than the inversion of H. It is, however, worthwhile noting that $BD_i\bar{B}^{-1}D_i^TB$ is not the standard discrete Laplace operator, but the so-called discrete pseudo-Laplacian, due to the interpolation operations between the GLL points and GL points implied in the derivative matrix D_i:

$$\text{GL points} \xrightarrow{D_i^TB} \text{GLL points} \xrightarrow{\bar{B}^{-1}} \text{GLL points} \xrightarrow{BD_i} \text{GL points}.$$

This fact will be pointed out again later to emphasize the interest of the $\mathbb{P}_N \times \mathbb{P}_N$ methods that we are going to introduce later in the paper.

2.2. $\mathbb{P}_N \times \mathbb{P}_{N-2}$ projection methods

Projection method was introduced in the late 1960's independently by Chorin [8,9] and Temam [27] as a way of computing the solutions of incompressible Navier-Stokes equations. Projection method is based on the following observation: In incompressible flows, the pressure is present only as a Lagrange multiplier for the incompressibility constraint. This observation motivated a time-splitting scheme which decouples the computation of the velocity and the pressure. In the first step, an intermediate velocity is computed using the momentum equation and ignoring the incompressibility constraint. In the second step, the intermediate velocity is projected to the divergence free space to get the next update of velocity and pressure. This procedure is more efficient than solving a coupled system of Stokes equations for velocity and pressure which would arise from a straightforward time discretization of the NSE (see Section 2.1).

The simplest form of the projection schemes looks like:

$$\begin{cases} \dfrac{1}{\triangle t}(\tilde{\boldsymbol{u}}^{n+1} - \boldsymbol{u}^n) - \nu\triangle\tilde{\boldsymbol{u}}^{n+1} = \boldsymbol{f}^{n+1}, \\ \tilde{\boldsymbol{u}}^{n+1}|_{\partial\Omega} = 0, \end{cases} \tag{2.15}$$

$$\begin{cases} \dfrac{1}{\triangle t}(\boldsymbol{u}^{n+1} - \tilde{\boldsymbol{u}}^{n+1}) + \nabla p^{n+1} = 0, \\ \nabla\cdot\boldsymbol{u}^{n+1} = 0, \boldsymbol{u}^{n+1}\cdot\boldsymbol{n}|_{\partial\Omega} = 0, \end{cases} \tag{2.16}$$

where $\boldsymbol{n}$ is the outward normal to $\partial\Omega$. It is seen that (2.16) implies the pressure boundary condition $\nabla p\cdot\boldsymbol{n} = 0$. This artificial Neumann boundary condition induces a numerical boundary layer that prevents the scheme to be fully first-order on the velocity in the H^1-norm and on the pressure in the L^2-norm, see, e.g., [23].

An improvement of the above non-incremental projection scheme was made by Goda [12, 28], who proposed to add the gradient of the previous pressure in the first step and

then accordingly correct the velocity in the second step:

$$\begin{cases} \dfrac{1}{2\triangle t}(3\tilde{\boldsymbol{u}}^{n+1}-4\boldsymbol{u}^{n}+\boldsymbol{u}^{n-1})-\nu\triangle\tilde{\boldsymbol{u}}^{n+1}+\nabla p^{n}=\boldsymbol{f}^{n+1}, \\ \tilde{\boldsymbol{u}}^{n+1}|_{\partial\Omega}=0, \end{cases} \tag{2.17}$$

$$\begin{cases} \dfrac{1}{2\triangle t}(3\boldsymbol{u}^{n+1}-3\tilde{\boldsymbol{u}}^{n+1})+\nabla(p^{n+1}-p^{n})=0, \\ \nabla\cdot\boldsymbol{u}^{n+1}=0, \boldsymbol{u}^{n+1}\cdot\boldsymbol{n}|_{\partial\Omega}=0. \end{cases} \tag{2.18}$$

This incremental projection scheme was then analyzed by several authors in different contexts. It has been proved that the scheme possesses second order accuracy for the velocity and first order accuracy for the pressure in the $l^{\infty}(L^2)$-norm, see, e.g., [11]. It is worthwhile mentioning that this scheme produces still a numerical boundary layer due to the non-physical Neumann boundary condition:

$$\nabla(p^{n+1}-p^{n})\cdot\boldsymbol{n}=0,$$

implied in the second sub-problem (2.18).

To remove the artificial pressure boundary condition in the standard form of the incremental projection scheme, Timmermans, Minev and Van De Vosse proposed a modified scheme in the paper [26], in which they added a divergence correction in the projection step (2.18):

$$\begin{cases} \dfrac{1}{2\triangle t}(3\boldsymbol{u}^{n+1}-3\tilde{\boldsymbol{u}}^{n+1})+\nabla\phi^{n+1}=0, \\ \nabla\cdot\boldsymbol{u}^{n+1}=0, \boldsymbol{u}^{n+1}\cdot\boldsymbol{n}|_{\partial\Omega}=0, \end{cases} \tag{2.19}$$

with $\phi^{n+1}=p^{n+1}-p^{n}+\nu\nabla\cdot\tilde{\boldsymbol{u}}^{n+1}$.

The introduction of the rotational term $\nu\nabla\nabla\cdot\tilde{\boldsymbol{u}}^{n+1}$ ensures the compatibility of pressure boundary conditions, consequently prevents the solution from developing a numerical boundary layer. The scheme (2.17) and (2.19), called now as the pressure-correction scheme in rotational form, was investigated successively by Guermond and Shen [15] in the semi-discrete form, and Huang and Xu [17] in the full-discrete form under the context of Legendre spectral method. It was proved that the scheme provides a second-order accuracy on the velocity and a 3/2-order accuracy on the pressure in the L^2-norm.

Here we will not go into the details about these theoretical results. However we will discuss in detail the implementation issues of the projection methods, since it seems to us that there is considerable amount of confusion in the choice of formulation and spectral space pair for the discrete velocity and pressure.

First, it is natural to consider a variational formulation corresponding to problem (2.17) as follows: find $\tilde{\boldsymbol{u}}\in H_0^1(\Omega)^d$ such that

$$\alpha(\tilde{\boldsymbol{u}},\boldsymbol{v})+\nu(\nabla\tilde{\boldsymbol{u}},\nabla\boldsymbol{v})=(\tilde{\boldsymbol{s}},\boldsymbol{v}),\quad\forall\boldsymbol{v}\in H_0^1(\Omega)^d, \tag{2.20}$$

where $\tilde{\boldsymbol{s}} = -\nabla p^n + \boldsymbol{f}^{k+1} + \frac{1}{2\Delta t}(4\boldsymbol{u}^k - \boldsymbol{u}^{k-1})$. Its spectral approximation reads then: find $\tilde{\boldsymbol{u}}_{\mathcal{N}} \in X_{\mathcal{N}}$ such that

$$\alpha(\tilde{\boldsymbol{u}}_{\mathcal{N}}, \boldsymbol{v}_{\mathcal{N}})_{\mathcal{N},GL} + \nu(\nabla\tilde{\boldsymbol{u}}_{\mathcal{N}}, \nabla\boldsymbol{v}_{\mathcal{N}})_{\mathcal{N},GL} = (\tilde{\boldsymbol{s}}, \boldsymbol{v}_{\mathcal{N}})_{\mathcal{N},GL}, \quad \forall \boldsymbol{v}_{\mathcal{N}} \in X_{\mathcal{N}},$$

or in the compact form:

$$a_{\mathcal{N}}(\tilde{\boldsymbol{u}}_{\mathcal{N}}, \boldsymbol{v}_{\mathcal{N}}) = (\tilde{\boldsymbol{s}}, \boldsymbol{v}_{\mathcal{N}})_{\mathcal{N},GL}, \quad \forall \boldsymbol{v}_{\mathcal{N}} \in X_{\mathcal{N}}, \tag{2.21}$$

with $a_{\mathcal{N}}(\cdot,\cdot)$ defined in (2.7).

The key issue relies on how to solve the correction step (2.19). To our knowledge, there exist two ways to build the variational formulation for problem (2.19), which is indeed a so-called Darcy problem. Azaiez et al. [1] proposed a mixed formulation to the Darcy problem: find $(\boldsymbol{u}, \phi) \in H_0(div, \Omega) \times L_0^2(\Omega)$, such that

$$\begin{aligned} &\alpha(\boldsymbol{u}, \boldsymbol{v}) - (\nabla \cdot \boldsymbol{v}, \phi) = \alpha(\tilde{\boldsymbol{u}}, \boldsymbol{v}), \quad \forall \boldsymbol{v} \in H_0(div, \Omega), \\ &(\nabla \cdot \boldsymbol{u}, q) = 0, \quad \forall q \in L_0^2(\Omega), \end{aligned}$$

where the space $H_0(div, \Omega)$ is defined by

$$H_0(div, \Omega) := \{\boldsymbol{v} \in L^2(\Omega)^d; \nabla \cdot \boldsymbol{v} \in L^2(\Omega), \boldsymbol{v} \cdot \boldsymbol{n} = 0 \text{ on } \partial\Omega\}.$$

Approximation problems can be constructed according to this formulation. However, in the frame of spectral methods, there are two difficulties related to the mixed formulation: 1) all vector functions of the space $H_0(div, \Omega)$ are required to satisfy the continuity of the normal component, which is inconvenient in practical implementation; 2) the well-known *inf-sup* condition associated to the bilinear form $(\nabla \cdot \boldsymbol{v}, q)$ requires a compatibility between the discrete velocity and pressure space. This means, as proven in [1], that the degree of polynomial approximation for the pressure must be taken two degrees lower than that for the velocity. This would also complicate the implementation.

An another variational formulation to problem (2.19) exists. It consists in finding $(\boldsymbol{u}, \phi) \in L^2(\Omega)^d \times H^1(\Omega)/R$, such that

$$\begin{cases} \alpha(\boldsymbol{u}, \boldsymbol{v}) + (\boldsymbol{v}, \nabla\phi) = \alpha(\tilde{\boldsymbol{u}}, \boldsymbol{v}), \quad \forall \boldsymbol{v} \in L^2(\Omega)^d, \\ (\boldsymbol{u}, \nabla q) = 0, \quad \forall q \in H^1(\Omega)/R. \end{cases} \tag{2.22}$$

Note that here the boundary conditions in (2.19) have been incorporated into the second equation of (2.22). The advantage of this formulation is that the verification of the *inf-sup* condition can be accomplished in a easy way. In fact, for all $q \in H^1(\Omega)/R$, we take $\boldsymbol{v}$ equal to ∇q, then

$$\frac{(\boldsymbol{v}, \nabla q)}{\|\boldsymbol{v}\|_0 |q|_1} \geq 1.$$

This means it holds

$$\inf_{q \in H^1(\Omega)/R} \sup_{\boldsymbol{v} \in L^2(\Omega)^d} \frac{(\boldsymbol{v}, \nabla q)}{\|\boldsymbol{v}\|_0 |q|_1} \geq 1. \tag{2.23}$$

Based on the formulation (2.22), we consider the following spectral approximation: find $\boldsymbol{u}_{\mathcal{N}} \in \mathbb{P}_{N,E}(\Omega)^d, \phi_{\mathcal{N}} \in Y_{\mathcal{N}}$, such that

$$\begin{cases} \alpha(\boldsymbol{u}_{\mathcal{N}}, \boldsymbol{v}_{\mathcal{N}})_{\mathcal{N},GL} + (\boldsymbol{v}_{\mathcal{N}}, \nabla\phi_{\mathcal{N}})_{\mathcal{N},GL}\alpha(\tilde{\boldsymbol{u}}_{\mathcal{N}}, \boldsymbol{v}_{\mathcal{N}})_{\mathcal{N},GL}, \quad \forall \boldsymbol{v}_{\mathcal{N}} \in \mathbb{P}_{N,E}(\Omega)^d, \\ (\boldsymbol{u}_{\mathcal{N}}, \nabla q_{\mathcal{N}})_{\mathcal{N},GL} = 0, \quad \forall q_{\mathcal{N}} \in Y_{\mathcal{N}}, \end{cases} \tag{2.24}$$

where $Y_{\mathcal{N}} := H^1(\Omega) \cap \mathbb{P}_{M,E}(\Omega)/R$, with M a positive integer. It can be proved that for any positive integer $M \leq N$, problem (2.24) is well-posed. In fact, as in the proof of (2.23), we can prove the following *inf-sup* condition for all $M, 0 < M \leq N$:

$$\inf_{q_{\mathcal{N}} \in H^1(\Omega)\cap\mathbb{P}_{M,E}(\Omega)/R} \sup_{\boldsymbol{v}_{\mathcal{N}} \in \mathbb{P}_{N,E}(\Omega)^d} \frac{(\boldsymbol{v}_{\mathcal{N}}, \nabla q_{\mathcal{N}})_{\mathcal{N},GL}}{\|\boldsymbol{v}_{\mathcal{N}}\|_0 |q_{\mathcal{N}}|_1} \geq 1. \tag{2.25}$$

For practical purposes, we take $\boldsymbol{v}_{\mathcal{N}} = \nabla q_{\mathcal{N}}$ in the first equation of (2.24), then we have, by using the second one, the following Poisson problem: find $\phi_{\mathcal{N}} \in Y_{\mathcal{N}}$, such that

$$(\nabla\phi_{\mathcal{N}}, \nabla q_{\mathcal{N}})_{\mathcal{N},GL} = \alpha(\tilde{\boldsymbol{u}}_{\mathcal{N}}, \nabla q_{\mathcal{N}})_{\mathcal{N},GL}, \quad \forall q_{\mathcal{N}} \in Y_{\mathcal{N}}. \tag{2.26}$$

Once $\phi_{\mathcal{N}}$ is obtained, we compute $\boldsymbol{u}_{\mathcal{N}}$ trivially by substituting $\phi_{\mathcal{N}}$ to the first equation of (2.24).

From the point of view of the accuracy of pressure, it is desirable to use a value of M the biggest possible. Moreover, it is observed from the second equation of (2.24) that the bigger is M the more close to zero is the divergence of the discrete velocity field. Based on these observations, some authors have tried the so-called $\mathbb{P}_N \times \mathbb{P}_N$ space pair, corresponding to taking $M = N$ in (2.26) in their computation. Unfortunately, numerical pressure oscillations or loss of accuracy by using the $\mathbb{P}_N \times \mathbb{P}_N$ projection methods have been recently reported [2]. Although an explanation for that was given in [13] by considering a steady state solution, it seems to us that the real cause of the loss of accuracy is not yet clear. In fact it can be verified that the spurious modes presented in a $\mathbb{P}_N \times \mathbb{P}_N$ scheme for the Stokes problem are excluded from the pressure in the projection step even if $M = N$. In our numerical experiments, we have found that the loss of accuracy of the $\mathbb{P}_N \times \mathbb{P}_N$ methods has different behaviors for different kinds of domains.

In Fig. 2, we plot the L^2- and H^1-velocity errors and L^2- and L^∞-pressure errors as functions of the time step size. It is observed that the pressure in both L^2 and L^∞ norms fails to converge when the time step decreases. The situation is somewhat improved in domains with smooth boundary. Fig. 3 presents the velocity and the pressure errors in the same norms as in Fig. 2. It is seen that the pressure computed in the circle domain remains convergent. We note however that the convergence rate decreases considerably with compared to the usual compatible approximations as we will see below. This suggests that the pressure oscillation caused by the equal-order velocity-pressure approximation may be related to the inconsistent pressure boundary conditions, especially when the domain includes corners. But it remains an open question how the domain corners affect the accuracy of the equal-order velocity-pressure approximation.

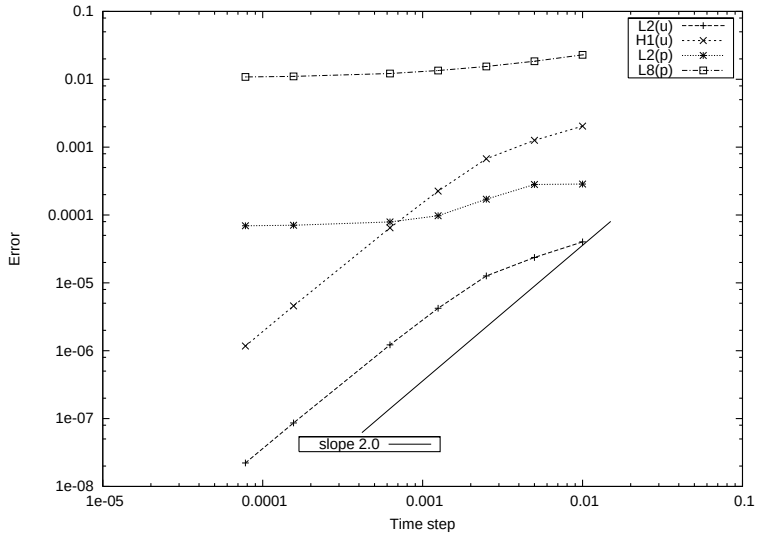

Figure 2: The velocity and pressure errors as functions of the time step by the $\mathbb{P}_N \times \mathbb{P}_N$ projection method in the square domain.

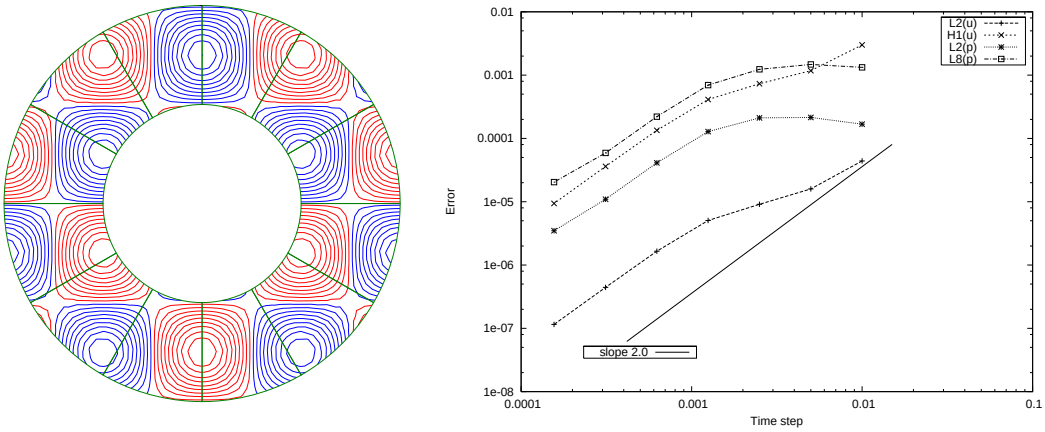

Figure 3: Left: Isolines of the solution in the smooth domain; Right: The velocity and pressure errors as functions of the time step in the smooth domain.

Due to these observations, people usually employ $\mathbb{P}_N \times \mathbb{P}_{N-2}$ velocity-pressure space pair in projection methods, although there exists $\mathbb{P}_N \times \mathbb{P}_N$ approaches in the velocity correction projection methods [13] in some cases. In a $\mathbb{P}_N \times \mathbb{P}_{N-2}$ projection method, one seeks in the second step to find $\boldsymbol{u}_{\mathcal{N}} \in \mathbb{P}_{N,E}(\Omega)^d, \phi_{\mathcal{N}} \in H^1(\Omega) \cap \mathbb{P}_{N-2,E}(\Omega)/R$, such that

$$\begin{cases} \alpha(\boldsymbol{u}_{\mathcal{N}}, \boldsymbol{v}_{\mathcal{N}})_{\mathcal{N},GL} + (\boldsymbol{v}_{\mathcal{N}}, \nabla\phi_{\mathcal{N}})_{\mathcal{N},GL} = \alpha(\tilde{\boldsymbol{u}}_{\mathcal{N}}, \boldsymbol{v}_{\mathcal{N}})_{\mathcal{N},GL}, \quad \forall \boldsymbol{v}_{\mathcal{N}} \in \mathbb{P}_{N,E}(\Omega)^d, \\ (\boldsymbol{u}_{\mathcal{N}}, \nabla q_{\mathcal{N}})_{\mathcal{N},GL} = 0, \quad \forall q_{\mathcal{N}} \in H^1(\Omega) \cap \mathbb{P}_{N-2,E}(\Omega)/R. \end{cases} \tag{2.27}$$

In Fig. 4, we present the result of a simple test using this approximation in the square domain, showing the second order convergence of the pressure for the rotational projection scheme and an order between 3/2 and 2 for the standard projection scheme. This means

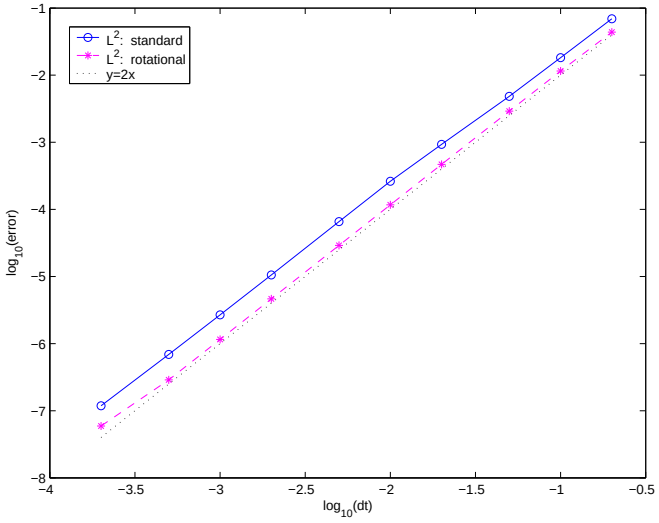

Figure 4: $\mathbb{P}_N \times \mathbb{P}_{N-2}$ projection scheme in the square domain.

that the estimates given in both [15] and [17] are not optimal for the pressure errors in some cases.

Concerning the computational complexity, in a manner similar to the $\mathbb{P}_N \times \mathbb{P}_{N-2}$ Uzawa approach in Section 2.1, we can obtain a matrix statement of the problems (2.21) and (2.27):

$$\begin{aligned}
&H\underline{\tilde{u}}_i = \bar{B}\tilde{s}_i, \quad i = 1, \cdots, d,\\
&\alpha\bar{B}\underline{u}_i + \bar{B}\tilde{D}_i\underline{\phi} = \alpha\bar{B}\underline{\tilde{u}}_i, \quad i = 1, \cdots, d,\\
&\tilde{D}_i^T\bar{B}\underline{u}_i = 0,\\
&\underline{p} = \underline{\phi} + \underline{p}^n,
\end{aligned}$$

or the equivalent form:

$$\begin{aligned}
&H\underline{\tilde{\boldsymbol{u}}} = \bar{B}\tilde{\boldsymbol{s}},\\
&\alpha^{-1}(\tilde{\boldsymbol{D}}^T\bar{B}\tilde{\boldsymbol{D}})\underline{\phi} = \tilde{\boldsymbol{D}}^T\bar{B}\underline{\tilde{\boldsymbol{u}}},\\
&\underline{\boldsymbol{u}} = \underline{\tilde{\boldsymbol{u}}} - \alpha^{-1}\tilde{\boldsymbol{D}}\underline{\phi},\\
&\underline{p} = \underline{\phi} + \underline{p}^n.
\end{aligned} \tag{2.28}$$

In the above systems, $\tilde{\boldsymbol{D}} := (\tilde{D}_1, \cdots, \tilde{D}_d)$ is the matrix form of the discrete gradient operator defined in the GLL$(N-2)$ points:

$$\begin{aligned}
(\tilde{D}_1)_{ijk,lmn} &:= \tilde{D}_{il}\tilde{I}_{jm}\tilde{I}_{kn},\\
(\tilde{D}_2)_{ijk,lmn} &:= \tilde{I}_{il}\tilde{D}_{jm}\tilde{I}_{kn},\\
(\tilde{D}_3)_{ijk,lmn} &:= \tilde{I}_{il}\tilde{I}_{jm}\tilde{D}_{kn},
\end{aligned}$$

where $(\tilde{D}_{pq})_{0\le p\le N, 1\le q\le N-1}, \tilde{D}_{pq} = \tilde{h}_q'(\xi_p)$, is the GLL$(N-2)\to$ GLL(N) derivative matrix, with $\tilde{h}$ the Lagrangian interpolants based on the GLL$(N-2)$ points. $(\tilde{I}_{pq})_{0\le p\le N, 1\le q\le N-1}$,

with $\tilde{I}_{pq} = \tilde{h}_q(\xi_p)$, is the interpolation matrix, mapping nodal values from GLL($N-2$) points to GLL(N) points. Note that in the projection methods of rotational form, the pressure updating should be replaced by

$$\underline{p} = \underline{\phi} + \underline{p}^n - \nu \tilde{B}^{-1} \tilde{\boldsymbol{D}}^T \bar{B} \underline{\boldsymbol{u}},$$

where $\tilde{B}$ is the GLL($N-2$) mass matrix. The main computational cost of (2.28) is the solution of a Poisson-like system on $\underline{\phi}$ and d Helmholtz systems on $\underline{\tilde{\boldsymbol{u}}}$. Usually, matrix $\tilde{\boldsymbol{D}}^T \bar{B} \tilde{\boldsymbol{D}}$ is much ill-conditioned than H, specially for computations with small time step and/or high Reynolds number. Consequently, it is the solution of the pressure increment $\underline{\phi}$ which is the most computational expensive. Now we make a comparison between this system on $\underline{\phi}$ and system (2.13). Firstly, two systems have nearly the same dimension. Secondly, due to the stiffness summation associated to the velocity continuity on the elemental interfaces, the evaluation of the matrix-vector multiplication $(B\boldsymbol{D}\bar{B}^{-1}\boldsymbol{D}^T B)\delta\underline{p}$ is more expensive than $(\tilde{\boldsymbol{D}}^T \bar{B} \tilde{\boldsymbol{D}})\underline{\phi}$. In the latter case some fast evaluation technique by combining $\tilde{\boldsymbol{D}}^T$ and $\tilde{\boldsymbol{D}}$ can be used to accelerate the matrix-vector multiplication. A precise cost estimate will be provided in the next section. Finally, our numerical tests show that the condition numbers of two systems are close to each other.

We note however that in multi-domain case Uzawa-based methods produce a continuous velocity field and a discontinuous pressure across the elemental interfaces, while projection-based methods give a discontinuous velocity field and a continuous pressure. This difference may play important role when the nonlinear convection terms are involved.

3. A $\mathbb{P}_N \times \mathbb{P}_N$ method

As we have seen in the previous section, both Uzawa-based $\mathbb{P}_N \times \mathbb{P}_{N-2}$ method and projection-based $\mathbb{P}_N \times \mathbb{P}_{N-2}$ method lead to a discrete pseudo-Laplace system for the pressure increment, i.e., system (2.13) or system on $\underline{\phi}$ in (2.28).

In this section, we aim at providing a $\mathbb{P}_N \times \mathbb{P}_N$ method for the Stokes equation. As we are going to see, the new method is simpler to implement, and cheaper in computational cost.

Let us start by re-examining the projection step in a projection-based method. From the viewpoint of implementation, unlike the methods where the velocity and the pressure are formulated in a coupled form, the LBB condition is not mandatory for the projection methods to work. In fact, in each time step two discrete sub-problems are well posed with any order of the pressure approximation no larger than the order of the velocity approximation. The numerical failure of the $\mathbb{P}_N \times \mathbb{P}_N$ projection method is not due to ill-posedness, but due to accumulation of the high frequency components in the pressure solution developing with the time step. This point is justified by the observation that the convergence failure occurs only in the late time of the computation. This motivates us to consider a filtering procedure, which consists in removing the last two modes in the pressure expansion. Precisely, in each time step we first solve the following $\mathbb{P}_N \times \mathbb{P}_N$ discrete problems

1) Diffusion step: find $\tilde{\boldsymbol{u}}_{\mathcal{N}} \in H_0^1(\Omega)^d \cap \mathbb{P}_{N,E}(\Omega)^d$ such that

$$a_{\mathcal{N}}(\tilde{\boldsymbol{u}}_{\mathcal{N}}, \boldsymbol{v}_{\mathcal{N}}) = (\tilde{\boldsymbol{s}}, \boldsymbol{v}_{\mathcal{N}})_{\mathcal{N},GL}, \quad \forall \boldsymbol{v}_{\mathcal{N}} \in H_0^1(\Omega)^d \cap \mathbb{P}_{N,E}(\Omega)^d;$$

2) Projection step: find $\boldsymbol{u}_{\mathcal{N}} \in \mathbb{P}_{N,E}(\Omega)^d, \phi_{\mathcal{N}} \in H^1(\Omega) \cap \mathbb{P}_{N,E}(\Omega)/R$, such that

$$\begin{cases} \alpha(\boldsymbol{u}_{\mathcal{N}}, \boldsymbol{v}_{\mathcal{N}})_{\mathcal{N},GL} + (\boldsymbol{v}_{\mathcal{N}}, \nabla\phi_{\mathcal{N}})_{\mathcal{N},GL} = \alpha(\tilde{\boldsymbol{u}}_{\mathcal{N}}, \boldsymbol{v}_{\mathcal{N}})_{\mathcal{N},GL}, \quad \forall \boldsymbol{v}_{\mathcal{N}} \in \mathbb{P}_{N,E}(\Omega)^d, \\ (\boldsymbol{u}_{\mathcal{N}}, \nabla q_{\mathcal{N}})_{\mathcal{N},GL} = 0, \quad \forall q_{\mathcal{N}} \in H^1(\Omega) \cap \mathbb{P}_{N,E}(\Omega)/R; \end{cases}$$

3) Updating step: update the pressure by

$$p_{\mathcal{N}} = \phi_{\mathcal{N}} + p_{\mathcal{N}}^n - \nu\nabla \cdot \tilde{\boldsymbol{u}}_{\mathcal{N}};$$

4) Post-filtering step: project the updated pressure $p_{\mathcal{N}}$ into $P_{N-2,E}$ space via the filter $F_{\mathcal{N}}$ defined by: $\forall q_{\mathcal{N}} \in \mathbb{P}_{N,E}(\Omega)$, $F_{\mathcal{N}} q_{\mathcal{N}} \in \mathbb{P}_{N-2,E}(\Omega)$, such that

$$(F_{\mathcal{N}} q_{\mathcal{N}})|_{\Omega_e} = \sum_{l,m,n=0}^{N-2} \hat{q}_{lmn}^e L_l(x_1) L_m(x_2) L_n(x_3), \tag{3.1}$$

$$\text{with } q_{\mathcal{N}}|_{\Omega_e} = \sum_{l,m,n=0}^{N} \hat{q}_{lmn}^e L_l(x_1) L_m(x_2) L_n(x_3), \quad e = 1, \cdots, E.$$

The post-filtering can be realized by a simple matrix-vector multiplication. We mention that there exist other filters to remove the instability of the pseudospectral methods [16].

In this method, all unknown, $\tilde{\boldsymbol{u}}_{\mathcal{N}}, \boldsymbol{u}_{\mathcal{N}}, \phi_{\mathcal{N}}$, and $p_{\mathcal{N}}$, are defined in a unique grid. This greatly simplifies the implementation. The matricial form of the above algorithm reads:

1) $H\underline{\tilde{\boldsymbol{u}}} = \bar{B}\tilde{\boldsymbol{s}}$;
2) $\alpha^{-1}(\bar{\boldsymbol{D}}^T \bar{B} \bar{\boldsymbol{D}})\underline{\phi} = \bar{\boldsymbol{D}}^T \bar{B} \underline{\tilde{\boldsymbol{u}}}$,
   $\underline{\boldsymbol{u}} = \underline{\tilde{\boldsymbol{u}}} - \alpha^{-1}\bar{\boldsymbol{D}}\underline{\phi}$;
3) $\underline{p} = \underline{\phi} + \underline{p^n} - \nu\bar{\boldsymbol{D}}^T \underline{\tilde{\boldsymbol{u}}}$;
4) $\underline{p} \to T_F \underline{p}$,

where T_F is the matrix representation of the filter $F_{\mathcal{N}}$.

A remarkable thing in this unique grid spectral solver is that the pressure computation, which is the most computational expensive in the resolution of the NSE, is reduced to a real Laplace system (step 2). In terms of the computational complexity, the gain by using this solver is considerable as compared to the usual $\mathbb{P}_N \times \mathbb{P}_{N-2}$ methods. In Table 1, we compare the elemental operation numbers needed to evaluate the matrix-vector multiplications $B\boldsymbol{D}\bar{B}^{-1}\boldsymbol{D}^T B\delta\underline{p}, (\tilde{\boldsymbol{D}}^T \bar{B} \tilde{\boldsymbol{D}})\underline{\phi}$, and $(\bar{\boldsymbol{D}}^T \bar{B} \bar{\boldsymbol{D}})\underline{\phi}$ when an iterative method is considered. It is observed that the evaluation of the standard Laplace operator can be 9 times faster than the pseudo-Laplacians in general 3D geometries.

Moreover, a numerical investigation shows that the standard Laplace system is much better conditioned than the pseudo-Laplace systems. In Table 2, we list the condition

Table 1: Elemental operation numbers of the discrete Laplace operator and the pseudo-Laplace operators.

Dimension	2D		3D	
element type	undeformed	deformed	undeformed	deformed
$\bar{\boldsymbol{D}}^T\bar{B}\bar{\boldsymbol{D}}$	$2N^3$	$4N^3$	$3N^4$	$6N^4$
$\tilde{\boldsymbol{D}}^T\bar{B}\tilde{\boldsymbol{D}}$	$4N^3$	$8N^3$	$9N^4$	$18N^4$
$B\boldsymbol{D}\bar{B}^{-1}\boldsymbol{D}^TB$	$8N^3$	$16N^3$	$18N^4$	$54N^4$

Table 2: Comparison on condition numbers of the discrete Laplace and pseudo-Laplace operators.

N	$B\boldsymbol{D}\bar{B}^{-1}\boldsymbol{D}^TB$	$\bar{\boldsymbol{D}}^T\bar{B}\bar{\boldsymbol{D}}$
6	14091.55	1496.87
8	41892.33	4308.65
10	98140.35	9966.41

numbers of different matrices constructed in a spectral element mesh given in Fig. 5. It is seen that the condition number of the standard spectral element discrete Laplacian is about 10 times smaller than the ones of the pseudo-Laplacians.

Now we perform an accuracy study. To this end we first consider the Stokes problem in the 2D domain $\Omega = (-1,1)^2$ with the analytical solution:

$$\begin{cases} u_1(x_1,x_2,t) = \sin(t)\sin(2\pi x_1)\cos(2\pi x_2), \\ u_2(x_1,x_2,t) = -\sin(t)\cos(2\pi x_1)\sin(2\pi x_2), \\ p(x_1,x_2,t) = \sin^2(t)\cos(\pi x_1)\sin(\pi x_2). \end{cases}$$

In this test, we take N large enough such that the spatial discretization errors are negligible as compared with the time discretization errors.

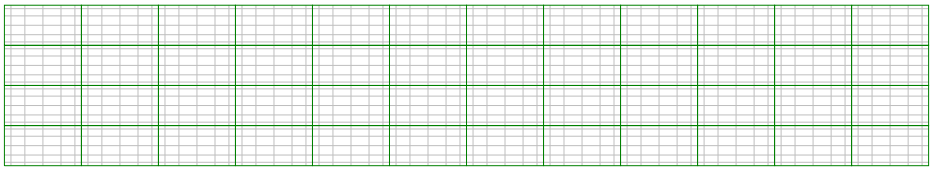

Figure 5: Example of spectral element mesh of a channel flow.

In Fig. 6, we plot, in log-log scale, the L^2-velocity and L^2-pressure errors with respect to $\triangle t$ for the Uzawa-based $\mathbb{P}_N \times \mathbb{P}_{N-2}$ method and the new $\mathbb{P}_N \times \mathbb{P}_N$ method. We observe that all errors decay as $\triangle t^2$, which means that the $\mathbb{P}_N \times \mathbb{P}_N$ method is stable, and as accurate as the classical $\mathbb{P}_N \times \mathbb{P}_{N-2}$ method.

It may be interesting to examine the error behavior in the L^∞ and H^1 norms. Fig. 7 shows the H^1-velocity and L^∞-pressure errors versus $\triangle t$. It is observed that the velocity accuracy in the H^1 norm remains the same, while the pressure convergence rate in the L^∞ norm for the $\mathbb{P}_N \times \mathbb{P}_N$ method is lower than second-order (close to $3/2$ order). It should be

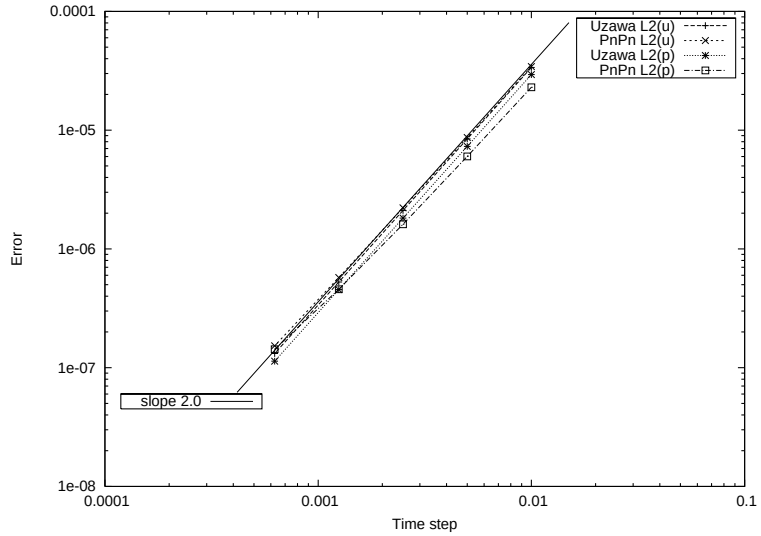

Figure 6: L^2-Error comparison between the Uzawa-based $\mathbb{P}_N \times \mathbb{P}_{N-2}$ method and $\mathbb{P}_N \times \mathbb{P}_N$ method.

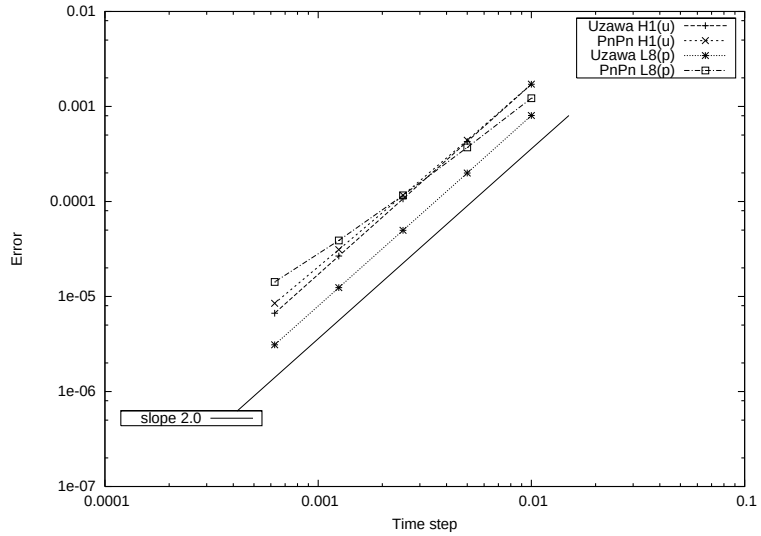

Figure 7: Same as in Figure 6, but in different norms.

noted that the loss of the pressure accuracy is not due to the equal-order velocity-pressure approximation, but the nature of the projection methods in the domains with corners. This point is confirmed by the next test in a smooth domain.

The above test is repeated in a circle domain with smooth boundary. In Figs. 8 and 9, we plot respectively the L^2-velocity and L^2-pressure errors, and the H^1-velocity and L^∞-pressure errors as functions of the time step. In these two figures we see that even more accurate (but with the same order) solutions have been obtained by the $\mathbb{P}_N \times \mathbb{P}_N$ method.

For the time being, we do not know how the smoothness of the domain boundary affects the convergence rate in time for the proposed method. We believe that this is

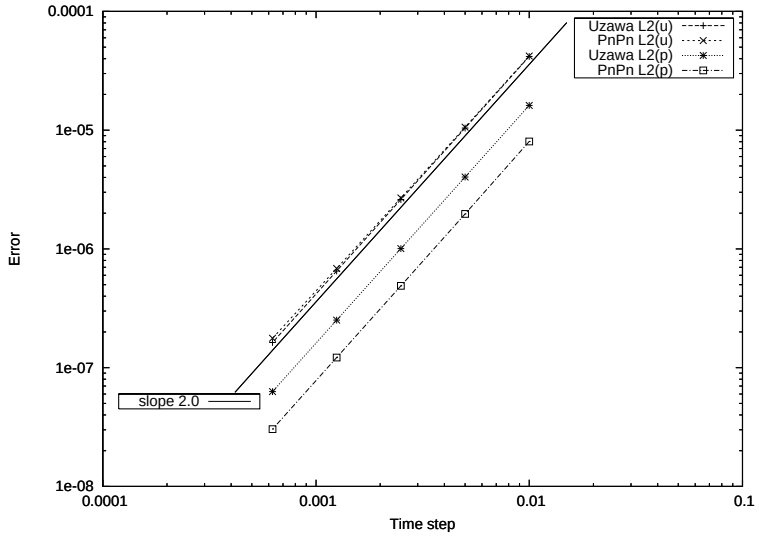

Figure 8: L^2-errors in the smooth domain.

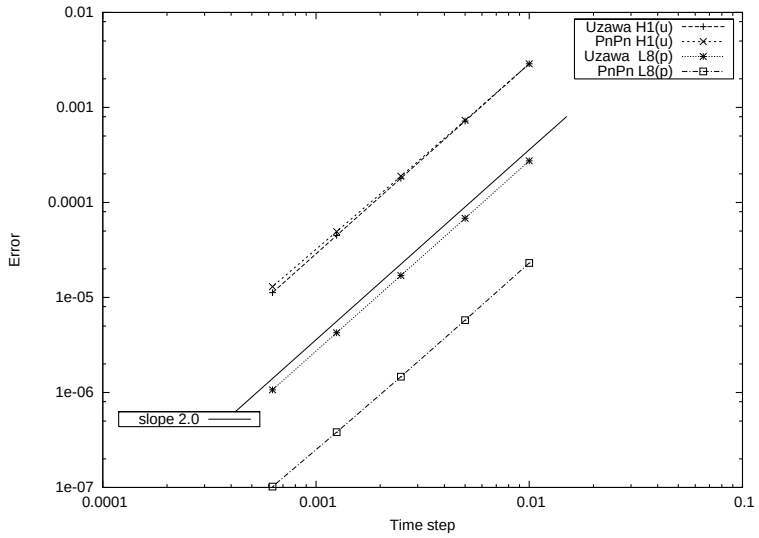

Figure 9: H^1 velocity errors and L^∞ pressure errors in the smooth domain.

not an easy question, and more investigation needs to be carried out to understand the cause behind this phenomena. It should be noted that the same phenomena occurs in all projection-type methods (see, e.g., [15]), in which it was proven that the convergence rate for the pressure is generally 3/2-order in square domains, while numerical experiments show the convergence of second order in the case of smooth domains. Our guess is that this phenomena may be related to the particular divergence distribution in the square domain. It is readily seen that the divergence of the intermediate velocity field at the corners is exactly zero (a particularity of the spectral method), while it allows a magnitude of order $\triangle t^2$ at the other grid-points. No null of the divergence may help in improving the

overall accuracy since the projection method can be regarded as an artificial compressibility technique.

In order to check the efficiency of the proposed $\mathbb{P}_N \times \mathbb{P}_N$ projection method for the unsteady incompressible Navier-Stokes equations, we perform one more numerical experiment to show the effects of the nonlinear terms in terms of CPU time. Note that although the nonlinear terms have no effect on the convergence rate in time, they certainly modify the overall computational complexity of the $\mathbb{P}_N \times \mathbb{P}_N$ method. In Table 3, we present the comparison result in terms of CPU time for different methods. In the calculation, the computational domain is a square with partition of 8 equal elements, a second order Adams-Bashforth scheme has been used to treat the convective terms. The conjugate gradient method is employed to solve both the pressure and the velocity systems. The computation is stopped at the time 1 with the time step fixed to 0.005. It is observed that the speed-up by using the $\mathbb{P}_N \times \mathbb{P}_N$ projection method ranges from 3 to 7 depending on the polynomial degree, and it increases as the polynomial degree increases.

Table 3: Comparison on CPU time in second.

N	$\mathbb{P}_N \times \mathbb{P}_{N-2}$ Uzawa/Factorization	$\mathbb{P}_N \times \mathbb{P}_N$ Projection
7	5.28	1.820
9	13.560	3.790
11	29.130	7.170
13	51.760	11.49
15	83.730	16.95
17	139.26	24.48
19	221.79	34.96
21	336.04	50.36
23	491.72	70.96
25	718.79	99.95

In summary, we have presented an efficient equal-order velocity-pressure spectral element approximation, say $\mathbb{P}_N \times \mathbb{P}_N$ method, for the Stokes equations. A detailed numerical comparison shows that the new method is stable, simpler to implement, and as accurate as the existing two grids methods, such as Uzawa-based $\mathbb{P}_N \times \mathbb{P}_{N-2}$ methods and projection-based $\mathbb{P}_N \times \mathbb{P}_{N-2}$ methods. Most importantly, use of the new $\mathbb{P}_N \times \mathbb{P}_N$ method significantly decreases the computational cost as compared to the well-known $\mathbb{P}_N \times \mathbb{P}_{N-2}$ methods for the Navier-Stokes equations.

Acknowledgments The research of the first author was partially supported by National NSF of China under Grant 10602049. The research of the second author was partially supported by National NSF of China under Grant 10531080, the Excellent Young Teachers Program by the Ministry of Education of China, and 973 High Performance Scientific Computation Research Program 2005CB321703.

References

[1] M. Azaiez, F. B. Belgacem, C. Bernardi, *Mortar spectral element discretization of Darcys equations*, Thirteenth International Conference on Domain Decomposition Methods, Editors: N. Debit, M.Garbey, R. Hoppe, J. Pąäeriaux, D. Keyes, Y. Kuznetsov, pp. 189-195 (2000).

[2] F. Auteri, J.L. Guermond, and N. Parolini, *Role of the LBB condition in weak spectral projection methods*, J. Comput. Phys., **420**, pp. 405-420 (2001).

[3] C. Bernardi, C. Canuto, Y. Maday, and B. Métivet, *Single-grid spectral collocation for the Navier-Stokes equations*, IMA J. Numer. Anal., **10**(2), pp. 253-297 (1990).

[4] C. Bernardi, Y. Maday, *Approximations spectrales de problèmes aux limites elliptiques*, Springer-Verlag, Paris, 1992.

[5] F. Brezzi, *On the existence, uniqueness and approximation of saddle-point problems arising from Lagrangian multipliers*, RAIRO, **8**, pp. 129-151 (1974).

[6] C. Canuto, M.Y. Hussaini, A. Quarteroni, T.A. Zang, *Spectral Methods in Fluid Dynamics*, Springer Verlag, New York, 1988.

[7] W. Couzy, *Spectral Element Discretization of the Unsteady Navier-Stokes Equations and its Iterative Solution on Parallel Computers*, PhD thesis, Swiss Federal Institue of Technology-Lausanne, 1995. Thesis no. 1380.

[8] A.J. Chorin, *Numerical solution of the Navier-Stokes equations*, Math. Comp., **22**, pp. 464-499 (1968).

[9] A.J. Chorin, *On the convergence of discrete approximations to the Navier-Stokes equations*, Math. Comp., **23**, pp. 341-353 (1969).

[10] P. Fischer, *An overlapping Schwarz method for spectral element solution of the incompressible Navier-Stokes equations*, J. Comput. Phys., **133**, pp. 84-101 (1997).

[11] J.L. Guermond, *Un résultat de convergence d'order deux en temps pour l'approximation des équations de Navier-Stokes par une technique de projection*, Modél. Math. Anal. Numér., **33**(1), pp. 169-189 (1999).

[12] K. Goda, *A multistep technique with implicit difference schemes for calculating two- or three-dimensional cavity flows*, J. Comput. Phys., **30**, pp. 76-95 (1979).

[13] J.L. Guermond, P. Minev, J. Shen, *An overview of projection methods for incompressible flows*, Comput. Methods Appl. Mech. Eng., **195**(44-47), pp. 6011-6045 (2006).

[14] J.L. Guermond, L. Quartapelle, *On stability and convergence of projection methods based on pressure Poisson equations*, Inter. J. Numer. Methods Fluids, **26**(9), pp. 1039-1053 (1998).

[15] J.L. Guermond, J. Shen, *On the error estimates for the rotational pressure-correction projection methods*, Math. Comp., **73**, pp. 1719-1737 (2004).

[16] D. Gottlieb, S.A. Orszag, and E. Turkel, *Stability of pseudospectral and finite-difference methods for variable coefficient problems*, Math. Comp., **37**(156), pp. 293-305 (1981).

[17] F.H. Huang, C.J. Xu, *On the error estimates for the rotational pressure-correction projection spectral methods for the unsteady Stokes equations*, J. Comput. Math., **23**(3), pp. 285-304 (2005).

[18] G.E. Karniadakis, M. Israeli, S.A. Orszag, *High-order splitting schemes for the incompressible Navier-Stokes equations*, J. Comput. Phys., **97**, pp. 414-443 (1991).

[19] Y.M. Lin, C.J. Xu, *A fractional step method for the unsteady viscous/inviscid coupled equation*, Advances in Scientific Computing and Applications, Y. Lu, W. Sun, T. Tang (Eds.), Science Press, pp. 286-295 (2004).

[20] Y. Maday, D. Meiron, A.T. Patera, E.M. Ronquist, *Analysis of iterative methods for the steady and unsteady Stokes problem: Application to spectral element discretization*, SIAM J. Sci. Comput., **14**(2), pp. 310-337 (1993).

[21] Y. Maday, A.T. Patera, *Spectral element methods for the incompressible Navier-Stokes equations*, State-of-the-art surveys in computational mechanics, A.K. Noor (ed.), ASME, New York, 1988, pp. 71-143.
[22] J.B. Perot, *An analysis of the fractional step method*, J. Comput. Phys., **108**, pp. 51-58 (1993).
[23] R. Rannacher, *On Chorin's projection method for the incompressible Navier-Stokes equations*, Lecture Notes in Mathematics, Springer, Berlin, pp. 167-183 (1992).
[24] J. Shen, *On pressure stabilization method and projection method for unsteady Navier-Stokes equations*, Advances in Computer Methods for Partial Differential Equations, IMACS, R. Vichnevetsky, D. Knight, G. Richter (ed.), pp. 658-662 (1992).
[25] J.C. Strikwerda, Y.S. Lee, *The accuracy of the fractional step method*, SIAM J. Numer. Anal., **37**(1)(electronic), pp. 37-47 (1999).
[26] L.J.P. Timmermans, P.D. Minev, F.N. Van De Vosse, *An approximate projection scheme for incompressible flow using spectral elements*, Inter. J. Numer. Meth. Fluids, **22**, pp. 673-688 (1996).
[27] R. Temam, *Sur l'approximation de la solution des équations de Navier-Stokes par la méthode des pas fractionnaires II*, Arch. Rat. Mech. Anal., **33**, p377-385 (1969).
[28] J. van Kan, *A second-order accurate pressure-correction scheme for viscous incompressible flow*, SIAM J. Sci. Stat. Comput., **7**(3), pp. 870-891 (1986).
[29] C.J. Xu, Y.M. Lin, *Analysis of iterative methods for the viscous/inviscid coupled problem via a spectral element approximation*, Inter. J Numer. Meth. Fluids, **32**, pp. 619-646 (2000).